fire

MDPI

Article

Comparative Study of Longitudinal Temperature Decay of Weak and Strong Plumes with Different Tunnel Aspect Ratios

Zhisheng Li [1], Xin Liu [1], Yanying Cheng [2], Gang Li [3,4], Dong Xu [1], Wei Hou [1,*], Rui Zheng [1] and Baiyi Li [2,*]

[1] School of Mining and Geomatics Engineering, Hebei University of Engineering, Handan 056038, China; lzsfire@163.com (Z.L.); lx17730707852@163.com (X.L.); cumtxudong@cumt.edu.cn (D.X.); zhengrui@hebeu.edu.cn (R.Z.)
[2] Chengdu Fire Protection and Rescue Research Center, Chengdu 610405, China; yanyingb7152@163.com
[3] State Key Laboratory of Safety and Health for Metal Mine, Maanshan 243000, China; ligang3@sinosteel.com
[4] Sinosteel Maanshan General Institute of Mining Research Co., Ltd., Maanshan 243000, China
* Correspondence: houwei@hebeu.edu.cn (W.H.); baiyi456@hotmail.com (B.L.)

Abstract: Numerical investigations were performed to compare and analyze the effect of the tunnel aspect ratio on the temperature distribution caused by weak and strong plumes. Four tunnel aspect ratios were chosen, which were one, two, four, and eight, respectively. The heat release rates were manipulated within the range of 3 MW to 50 MW in order to replicate fire situations involving small cars, trucks, and big freight vehicles. The study revealed that the aspect ratio of the tunnel has minimal impact on the temperature distribution in the vicinity of the fire area, but it significantly affects the temperature distribution in the distant area from the fire source. The temperature gradient of the fire source at a distance exhibits a non-monotonic tendency in the far-field. The temperature distribution gradient decreases more significantly when driven by a strong plume compared to a weak plume. A quantified investigation of the maximum excess temperature was conducted by including a specific diameter for the fire source. Subsequent correlations of the longitudinal temperature distribution were established for both weak and strong plumes.

Keywords: tunnel aspect ratio; the maximum excess temperature; longitudinal temperature distribution; weak plume; strong plume

check for updates

Citation: Li, Z.; Liu, X.; Cheng, Y.; Li, G.; Xu, D.; Hou, W.; Zheng, R.; Li, B. Comparative Study of Longitudinal Temperature Decay of Weak and Strong Plumes with Different Tunnel Aspect Ratios. *Fire* **2024**, *7*, 431. https://doi.org/10.3390/fire7120431

Academic Editor: Lizhong Yang

Received: 2 October 2024
Revised: 4 November 2024
Accepted: 7 November 2024
Published: 25 November 2024

Copyright: © 2024 by the authors. Licensee MDPI, Basel, Switzerland. This article is an open access article distributed under the terms and conditions of the Creative Commons Attribution (CC BY) license (https://creativecommons.org/licenses/by/4.0/).

1. Introduction

Tunnel fires are likely to result in significant deaths and substantial economic damage due to the semi-enclosed nature of tunnels and their limited ability to dissipate heat. Additionally, the accumulation effect of flames and heated smoke will cause significant harm to the tunnel's construction. For instance, 189 people died, and about USD 500 billion was lost in direct economic losses in Korea Daegu Fire in 2003. Revisiting previous reports about tunnel fire accidents, smoke poisoning is an important cause of death [1]. When the flame height is lower than the tunnel height, the developed plume is called a weak plume in a tunnel fire. On the contrary, it is called a strong plume when the flame height exceeds the tunnel height [2,3]. A fire driven by a strong plume usually brings a greater threat to the tunnel's lining structures, devices, and passengers inside the tunnel than the weak plume. When a fire occurs in the building, it is necessary to start the ceiling temperature smoke detector in time to realize the rapid detection and alarm of the fire. Therefore, it is necessary to investigate the maximum temperature profile under the ceiling.

The study of temperature distribution is typically focused on investigating the formation of fire plumes in tunnel fires [4–8]. The temperature field, which encompasses the maximum excess temperature and the longitudinal temperature decline, has garnered significant attention in recent decades. The parameters generated by fire plumes in tunnel fires may be classified into two categories: weak plumes and strong plumes. The distinction between a weak plume and a strong plume was established based on the behavior of

the flame, as shown in Figure 1. The development process of a ceiling jet produced by weak and strong plumes exhibited distinct differences. The plume, propelled by thermal buoyancy, ascends and expands in a radial manner upon reaching the ceiling (Figure 1a,b). The turning zone is denoted by the crucial location $r = r_e$ [9,10]. However, a significant amount of energy was lost during the plume-turning process. The radiation heat loss for a strong plume is considerably more than that for a light plume in close proximity to the fire source [11]. The ceiling jet velocity u is the function of $(Q/H)^{1/3}$, and the coefficient value of 1.94 [3] for a weak plume is lower than that of 3.4 for a strong plume [12]. The Gaussian shape is frequently used to depict profiles of temperature rise and velocity as the distance increases. The plume center's temperature ΔT_0 excess is a function of $Q^{2/3}/(Z - Z_0)^{5/3}$. McCaffrey [13] provided another correlation to examine the disparity between the plume region and flame region in terms of the maximum excess temperature of the ceiling. Furthermore, the maximum temperature above the normal level remained stable inside the area where the heat was being released until the rate of heat release hit a specific threshold. As the heat release rate rose, the maximum excess temperature generated by a weak plume also increased. Once ignited, the fire plume transports diluted the fire byproducts mixed with entrained air toward the ceiling. The formation of the flame or smoke occurred under the ceiling and gradually increased in thickness and temperature over time. The fire environment was closely connected to the characteristics of this layer, which, in turn, was largely influenced by the rate at which the plume fluid entered the layer. The disparity between a weak and strong plume results in a non-dimensional constant of proportionality in the mass flow rate m correlation, as proposed in earlier research [14,15]. Overall, the variations in the plume characteristics parameter mentioned above result in distinct temperature distributions between weak and powerful plumes. More details about the ceiling jet being driven by weak and strong plumes can be found in Ref [15]. Hence, an examination was conducted to determine the highest temperature reached near the ceiling, taking into account different circumstances. Zhang et al. [16] investigated the effect of ceiling constriction on the temperature distribution driven by small and large fires. A correlation of the temperature distribution was modified based on McCaffrey's model [13]. Gao et al. [17] studied the maximum temperature distribution along the ceiling by taking sidewall constriction into account and proposed two formulas to develop the longitudinal and transverse temperature distributions driven by weak and strong plumes. Tang et al. [18] performed a further study on the effect of sidewall constriction and the fire source aspect ratio on the longitudinal temperature distribution. Consequently, a model was proposed by introducing the characteristic diameter of the fire source. Zhou et al. [19] studied the influence of the transverse fire source location on the temperature distribution driven by small and large fires in an arced ceiling tunnel. They found that McCaffrey's model underestimated the tested result due to the wall's confinement. This trend was also found by Li et al. [20] in a bifurcated tunnel fire.

Nevertheless, the majority of prior research on temperature distribution has been conducted in a specific cross-sectional tunnel, with only a small number of studies examining the impact of the tunnel aspect ratio on temperature distribution. It was observed that the tunnel aspect ratio is a critical factor that can have a substantial impact on the kinetic and thermodynamic characteristics. For instance, Ji et al. [21] reported that the smoke temperature deteriorated more rapidly as the contact area between the smoke and tunnel ceiling and the smoke layer increased in response to an increase in the aspect ratio. The smoke stratification thickness diminished as the tunnel aspect ratio increased, which implied that the smoke buoyancy head decreased [22]. Furthermore, a reduction in the critical velocity was found in Refs. [23,24]. In contrast, the aforementioned investigations were conducted in a tunnel with a maximal aspect ratio of 2.3. In recent years, advancements in infrastructure technology have led to the construction of ultra-wide cross-section tunnels, which serve to reduce traffic congestion. The Shenzhen–Zhongshan Link is situated in the Lingdingyang coastal region of the Pearl River Delta. The cross-sea waterway in question serves as a connection between Shenzhen City, Zhongshan City, and Guangzhou City in

China. The immersed tunnel was built to have a maximum width of 55.5 m and a height of 10.6 m, as shown in Figure 2. The tunnel's cross-section has an aspect ratio greater than 5.25. An additional contemporary illustration is the Lishui Road Tunnel project in Zhejiang [25], where the convergence zone exhibits an aspect ratio above eight. According to previous reports, the thickness of the smoke layer decreases as the tunnel width increases [22,26]. Consequently, the temperature field distribution is likely to be altered when the tunnel cross-section varies. Therefore, additional testing is required to determine the model's suitability for ultra-wide cross-section tunnels.

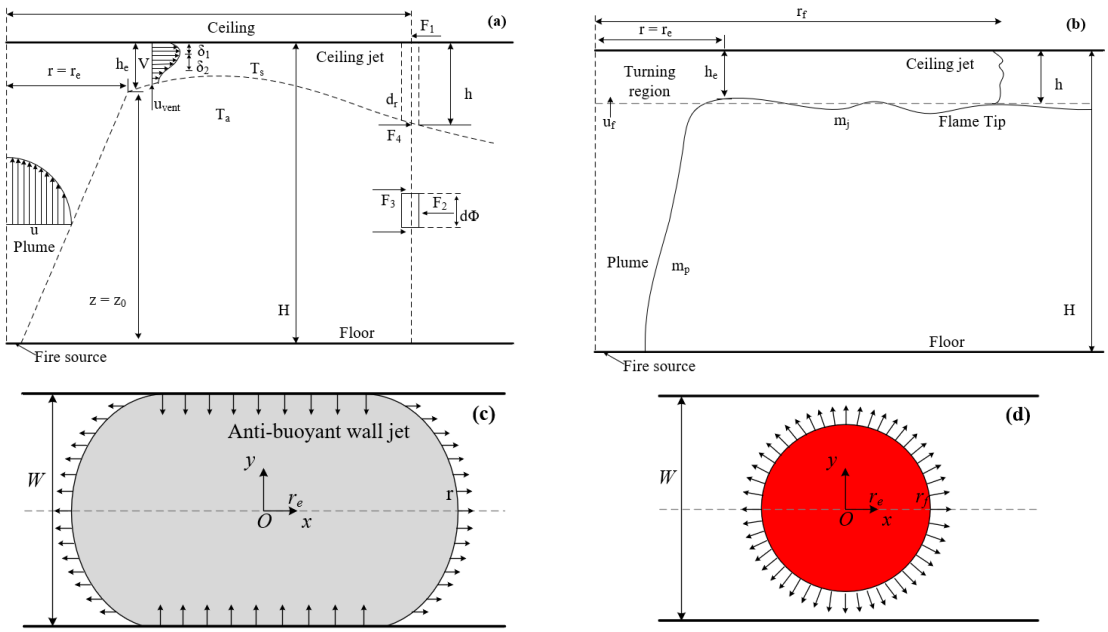

Figure 1. The schematic of a ceiling jet driven by a weak plume. (**a**) The side view redrawn by referring to [10] and (**c**) the top view. The strong plume (**b**) side view redrawn by referring to [9] and (**d**) the top view.



Figure 2. Shenzhen—Zhongshan Tunnel.

Consequently, a series of numerical simulations was performed to examine the impact of the tunnel aspect ratio on temperature distribution. The comparison of the temperature field driven by weak plume and strong plume was carried out. In addition, the correlation of temperature distribution was developed, which includes the maximum excess temperature and longitudinal temperature decay.

2. Numerical Methods

Due to the challenges in conducting physical tests with different tunnel aspect ratios, Fire dynamics simulator software (FDS 6.0) was used to simulate the flow caused by a

fire source in this work. The software numerically solves a variant of the Navier–Stokes equations, which is applicable to low-velocity flows (Ma < 0.3) driven by heat, with a particular focus on smoke and heat transfer during fire events. FDS incorporates two numerical methods: a large eddy simulation (LES) and direct numerical simulation (DNS) [27]. The LES method was selected in this work. The LES method was selected for this study. The filter function is essential in a large eddy simulation (LES) as it differentiates between large and small eddies. In this methodology, the large eddy is resolved directly through numerical calculations, while the small eddy is managed using Sub-Grid Models (SGMs).

The conservation of mass equation can be written as follows:

$$\frac{\partial \rho}{\partial t} + \nabla \cdot \rho u = 0 \tag{1}$$

The conservation of momentum equation is as follows:

$$\frac{\partial}{\partial t}(\rho u) + \nabla \cdot \rho u u + \nabla p = \rho g + f + \nabla \cdot \tau_{ij} \tag{2}$$

The conservation of energy equation is as follows:

$$\frac{\partial}{\partial t}(\rho h) + \nabla \cdot \rho h u = \frac{Dp}{Dt} + \dot{q}^{*''} - \nabla \dot{q}^{*\prime} + \Phi \tag{3}$$

Eddy viscosity is derived from the assumption that small scales are in equilibrium, which is achieved by balancing energy production and dissipation. The turbulent viscosity defined in FDS is as follows:

$$u_{LES} = \rho (C_S \Delta)^2 \left[\frac{1}{2} \left(\nabla \mu + \nabla \mu^T \right) \left(\nabla \mu + \nabla \mu^T \right) - \frac{2}{3} \nabla \mu^2 \right]^{1/2} \tag{4}$$

Moreover, it has been largely applied to fire safety areas, and validations of the FDS modeling of tunnel fires have been made against many experimental studies [28–34]. For instance, longitudinal temperature distribution under the tunnel ceiling in a tunnel fire, as simulated by FDS and observed in full-scale experiments, was found to be in good agreement, according to Zhang's work [31]. Simulation findings using FDS are in good agreement with experimental data, according to Wang's study [30], which compared the time-dependent temperature at a measurement location under the ceiling surrounding the fire source in a full-scale tunnel fire with the results. In addition, the maximum temperature simulation results under the ceiling were compared with the experimental results in our previous research work, where good consistency was obtained [33].

2.1. Tunnel Model

A full-scale tunnel model of 100 m was built in FDS, as shown in Figure 3. According to the actual tunnel surveys [35,36], the tunnel height was fixed to 5.5 m. An ultra-wide cross-section tunnel, like the Lishui Road Tunnel, has an aspect ratio greater than 8, as mentioned in the Section 1. Aspect ratios of 1, 2, 4, and 8 were used in this study to examine the impact of the aspect ratio on the temperature field. The tunnel widths used in the investigation ranged from 5 to 40 m. The ceiling and sidewalls were made of "CONCRETE" with a density of 2280 kg/m^3, a specific heat capacity of 1.04 kJ/(kg·K), and thermal conductivity of 1.8 W/(m. K) [35]. Twenty degrees Celsius is the baseline for the surrounding temperature.

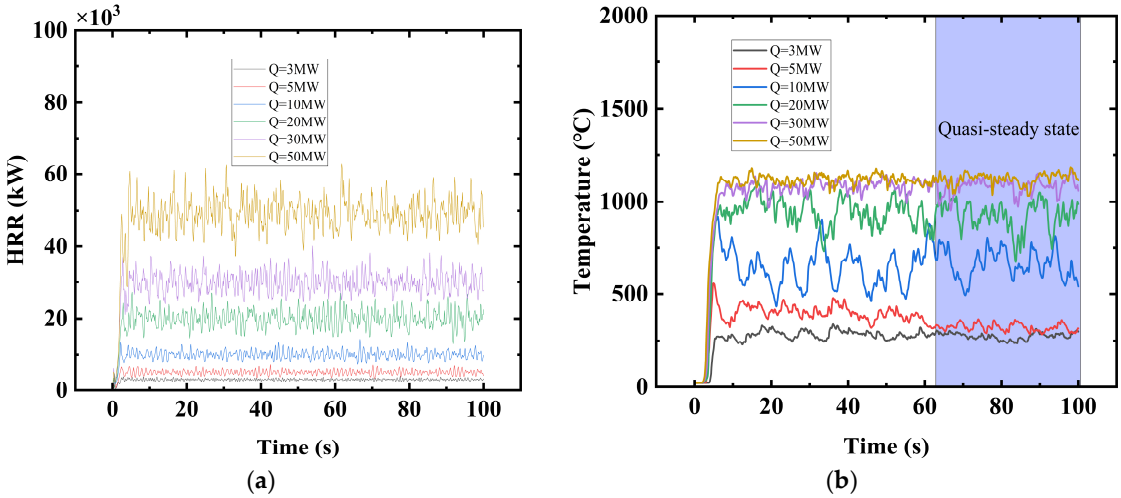

Figure 3. HRR and temperature verses time with different fire sources. (**a**) HRR versus time. (**b**) Temperature versus time.

2.2. Fire Scenarios

According to [37], the fire heat release rate (HRR) was designed at 3, 5, 10, 15, 20, 30, and 50 MW, taking into account the most common fire circumstances involving small cars (3~5 MW), trucks (10~20 MW), and heavy goods vehicles (30~50 MW) in road tunnels. The simulations were run for a maximum of 100 s. Diesel oil has been used as a fuel for fire. The heat release rate in the fire simulation is determined by the fire source area and heat release rate per unit area (command "HRRPUA" provided in FDS). In the present study, a square fire source area was established at 4 m², with varying heat release rates per unit area (HRRPUA) corresponding to different heat release rates. Furthermore, this research deliberately omits the early fire growth stage in the simulation, initiating the fire heat release rate from 0 MW and reaching the peak heat release rate within 3 s, after which it remains constant for a designated period. HRR curves corresponding to various fire source and tunnel aspect ratios are presented in Figure 3a. It is evident that all heat release rates align well with the actual simulation values and satisfy the current simulation requirements. A single-step simple chemistry combustion model was employed, with the carbon monoxide and soot yields for propane set at CO_YIELD = 0.005 and SOOT_YIELD = 0.024, respectively, in an REAC line of the fire dynamics simulator (FDS) code, respectively [15]. A similar setup in tunnel fires was also found in previous reports [38]. The average temperature was obtained in the purple region of Figure 3b. In terms of the intervals of the thermocouples, the near-field thermocouple spacing was 0.25 m, while the far-field spacing was 0.5 m. The temperature measuring points are illustrated in Figure 4.

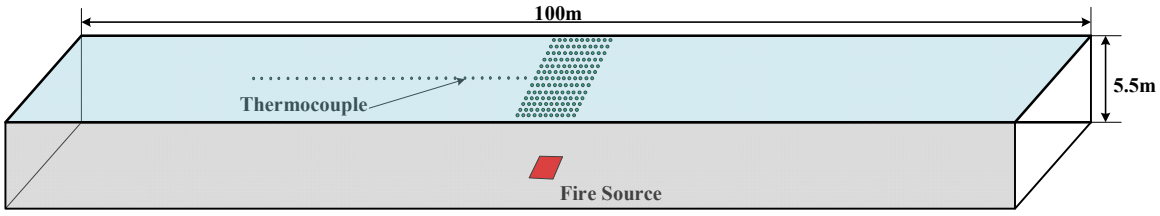

Figure 4. Schematic of tunnel model.

2.3. Grid Independence Analysis

The mesh size δx is a crucial parameter that guarantees the accuracy and dependability of the simulation. The characteristic diameter D^* is a crucial factor in determining the size

of the mesh, as indicated by Equation (5). The FDS user's handbook [27] suggests that the ratio of D^* to δx should fall between the range of 4 and 16, as described by Equation (6).

$$D^* = \left(\frac{Q}{\rho_\infty T_\infty c_p g^{1/2}} \right)^{2/5} \tag{5}$$

$$4 \leq \frac{D^*}{\delta x} \leq 16 \tag{6}$$

where ρ_∞ is the ambient air density, T_∞ is the ambient temperature, c_p is the specific heat capacity, and g is the acceleration of gravity. The suggested grid size range was around 0.22~0.90 m, and the characteristic fire diameter was 3.58 m, using an HRR of 3 MW as an example. To facilitate the comparison, four grid sizes ranging from 0.22 m to 0.5 m were used. Figure 5 displays the longitudinal temperature distribution along the ceiling. The tendency towards more homogeneous temperature curves is seen when the grid size is reduced. With a grid size of less than 0.25 m, the computing time increased without a discernible benefit. Consequently, a grid size of 0.25 m was used.

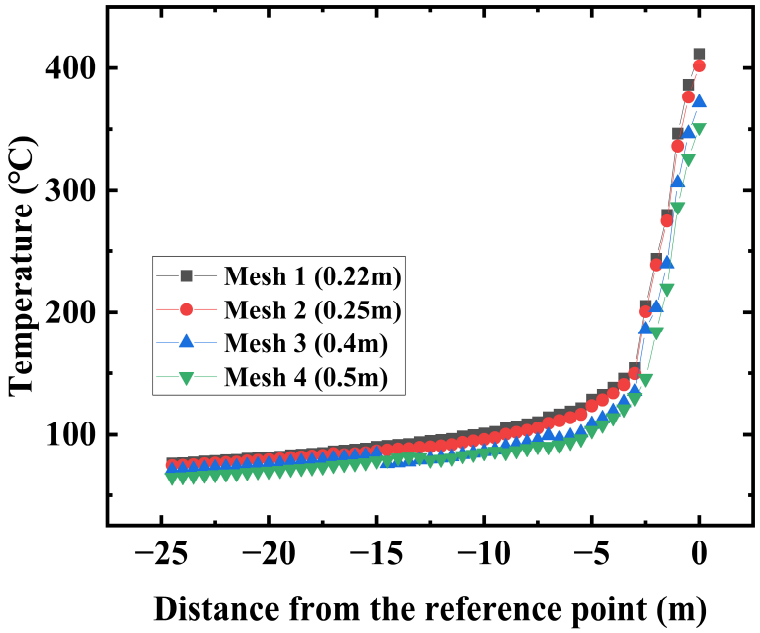

Figure 5. Grid independence analysis.

3. Results and Discussion

3.1. Ceiling Temperature Distribution Characteristics

Figure 6 depicts the effect of the tunnel aspect ratio (AR) on ceiling temperature distributions with two types of typical working conditions, where a weak plume scenario was simulated using HRR at 5 MW, and a strong plume scenario was represented by using HRR at 50 MW. It can be seen from Figure 6 that the temperature near the fire source varies somewhat with AR, but there is a significant variance in the distant field of the fire. This issue is significantly more visible in the case of a strong fire plume. The reason for this is that a large buoyancy effect was generated in the field near the fire source, whilst a relative buoyancy effect was caused in the field farther away. As a result, relatively little smoke accumulated on the far fire source field. Furthermore, the height of the flame rises in proportion to the increase in the heat release rate (HRR), resulting in a significant increase in thermal radiation [11]. Simultaneously, the heat loss from flame radiation exceeds the heat loss from smoke radiation, leading to a significant variation in the temperature gradient as the distance increases.

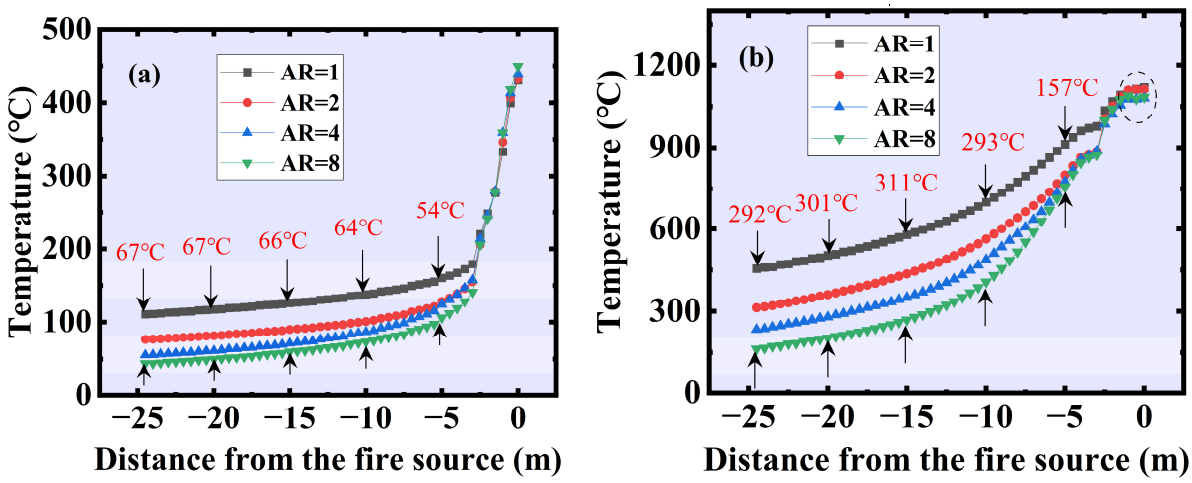

Figure 6. Effects of tunnel aspect ratios on the ceiling temperature distributions with two typical HRRs: (**a**) Q = 5 MW and (**b**) Q = 50 MW.

Upon further examination of the temperature distribution in both weak and strong plumes, it is evident that the temperature remains almost constant around the fire source in the strong plume fire scenario. This is indicated by the black dotted box in Figure 6b. The temperature measured in this area is the flame temperature, which is the reason for this. In addition, the influence of the tunnel's aspect ratio on the temperature of the far-field area surrounding the fire source is significant. This phenomenon occurs in both weak and strong plume circumstances, and it is notably prominent in the strong plume scenarios. As an illustration, the tunnel's aspect ratio results in a ceiling temperature that can reach a maximum departure of 54 °C (157 °C) for weak (strong) plumes. This discrepancy happens at a distance of 5 m away from the fire source. Furthermore, the temperature deviations display a non-monotonic pattern of fluctuation with increasing distance. Such quantified details of longitudinal temperature decay will be explored later.

3.2. The Maximum Excess Temperature

The flame reaches the ceiling with the increase in the heat release rate, and the ceiling jet flows from the pure plume to the entrained flame, hitting the ceiling until the flame spreads under the ceiling. According to McCaffrey's studies in an open space [13], the plume was divided into three regions, and the maximum excess temperature correlation was derived.

$$\frac{\Delta T_{\max}}{T_\infty} = \left(\frac{\varepsilon}{0.9\sqrt{2g}}\right)^2 \left(\frac{Z}{Q^{2/5}}\right)^{2\eta-1} \tag{7}$$

where $\Delta T_{\max}$ is the maximum excess temperature, ε is the constant, and Z is the distance from the fire source surface. A model for predicting the maximum excess temperature in a tunnel fire, which was created by Ji et al. [39] based on McCaffrey's correlation, divides the area into two parts based on the temperature's evolution behavior: the continuous flame zone and the non-continuous flame region; see Equation (8).

$$\frac{\Delta T_{\max}}{T_\infty} = \begin{cases} 43.69 \frac{Q^{*\prime 2/5} \cdot D}{H_{\text{ef}}}, \frac{Q^{*\prime 2/5} \cdot D}{H_{\text{ef}}} \leq 1.61 \\ 53, \frac{Q^{*\prime 2/5} \cdot D}{H_{\text{ef}}} > 1.61 \end{cases} \tag{8}$$

where H_{ef} is the effective height, $D = 2AB/(A+B)$ is the diameter of the fire source, A and B are the side length of the rectangular fire source, and $Q^{*\prime} = Q/\left(\rho_\infty T_\infty c_p g^{1/2} A B^{3/2}\right)$ is the dimensionless heat release rate.

A comparison of the simulated result with previous models predicted by Ji et al. [39] and McCaffrey [13] was conducted, as shown in Figure 7. The observed trend of the

obtained value in this work is consistent with earlier findings. The obtained result is marginally more than Ji's anticipated value, possibly due to variations in the thermal physical properties of the tunnel. The tested result exceeds the value anticipated by McCaffrey. The current scenario involves the transfer of heat from the wall back to the fire source within the confined space underneath the wall. In this work, we would like to develop another model of the maximum excess temperature. In addition, a characteristic diameter was used to previously quantify the fire behavior for weak and strong plumes [9,40]. Therefore, the fire source characteristic diameter D' was introduced to quantify the maximum excess temperature under the ceiling, which can be expressed as follows:

$$D' = \sqrt{4S/\pi} \tag{9}$$

where S is the area of the fire source. Thus, by substituting Equation (9) into Equation (8), the modified maximum excess temperature correlation can be written as follows:

$$\frac{\Delta T_{\max}}{T_\infty} = \begin{cases} \alpha \frac{Q^{*''2/5} \cdot D'}{H_{ef}}, \frac{Q^{*''2/5} \cdot D'}{H_{ef}} \le \lambda \\ \beta, \frac{Q^{*''2/5} \cdot D'}{H_{ef}} > \lambda \end{cases} \tag{10}$$

$$Q^{*''} = Q/\left(c_p \rho_\infty T_\infty g^{1/2} D'^{5/2}\right) \tag{11}$$

where $Q^{*''}$ is the dimensionless heat release rate and α, β, and λ are constants, which can be obtained by fitting the tested data. Figure 8 displays the non-dimensional maximum excess temperature as a function of the product of the non-dimensional heat release rate and characteristic diameter. A two-stage function was derived, with a critical value of 1.61. When $\frac{Q^{*''2/5} \cdot D'}{H_{ef}}$ exceeds 1.61, there is no correlation between $\frac{\Delta T_{\max}}{T_\infty}$ and $\frac{Q^{*''2/5} \cdot D'}{H_{ef}}$. On the other hand, $\frac{\Delta T_{\max}}{T_\infty}$ increases positively with the increase in $\frac{Q^{*''2/5} \cdot D'}{H_{ef}}$, as $\frac{Q^{*''2/5} \cdot D'}{H_{ef}}$ is less than 1.61. Consequently, the final expression of the maximum excess temperature can be written as follows:

$$\frac{\Delta T_{\max}}{T_\infty} = \begin{cases} 2.91 \frac{Q^{*''2/5} \cdot D'}{H_{ef}}, \frac{Q^{*''2/5} \cdot D'}{H_{ef}} \le 1.61 \\ 3.52, \frac{Q^{*''2/5} \cdot D'}{H_{ef}} > 1.61 \end{cases} \tag{12}$$

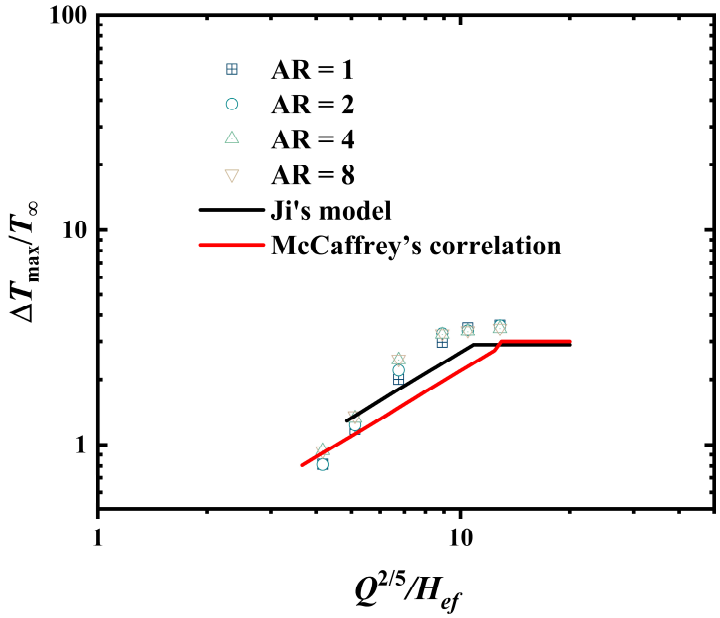

Figure 7. Comparison of the obtained result by FDS with previous correlations [13,39].

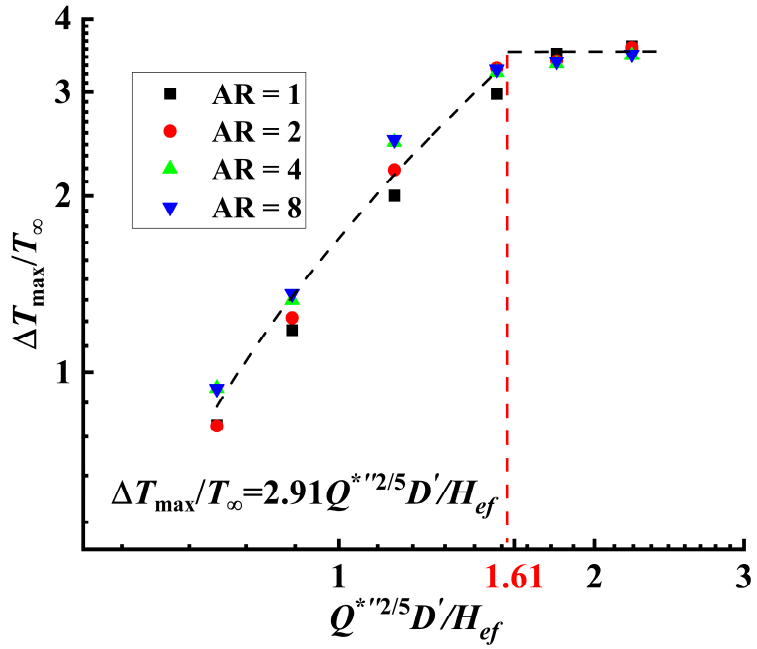

Figure 8. The non-dimensional maximum excess temperature correlations.

3.3. Longitudinal Temperature Decay Law

The longitudinal temperature distribution for weak and powerful fire plumes with varying tunnel aspect ratios has not been extensively explored, as mentioned in the Section 1. Upon reviewing past research, it was shown that longitudinal temperature decreases in an exponential manner as the distance from the place of ignition increases. Our objective was to establish a correlation between the longitudinal temperature distribution driven by the weak and strong plumes, considering the tunnel's cross-section. Therefore, the longitudinal temperature decay relationship is assumed as follows:

$$\frac{\Delta T_x}{\Delta T_{\max}} = Ae^{-Bx} + C \tag{13}$$

where ΔT_x is the longitudinal temperature excess along the tunnel ceiling, and x is the distance from the reference point. The decay coefficients A, B, and C are constants, which are related to the tunnel cross-section parameters. Thus, a function about the decay coefficient can be reasonably written as follows:

$$\Psi(i) = f(AR, Q) \tag{14}$$

Figure 9 displays the non-dimensional longitudinal temperature as a function of the non-dimensional distance from the reference point. The data used in this study were collected in a setting with natural ventilation. Therefore, the aforementioned fire source center was chosen as the designated site of reference. The height of the tunnel was chosen as the characteristic parameter to convert the longitudinal distance into a dimensionless quantity. The analysis of Figure 9 reveals that the decay rates of dimensionless longitudinal temperature for weak plumes exhibit minimal variation with the heat release rate. By contrast, the decay rate of dimensionless longitudinal temperature for powerful plumes displays a substantial divergence with the heat release rate. Consequently, the impact of the heat release rate on the decrease in temperature along the length of weak plumes may be disregarded, but it should be taken into account for strong plumes. Further elaboration on these specifics will be provided hereafter.

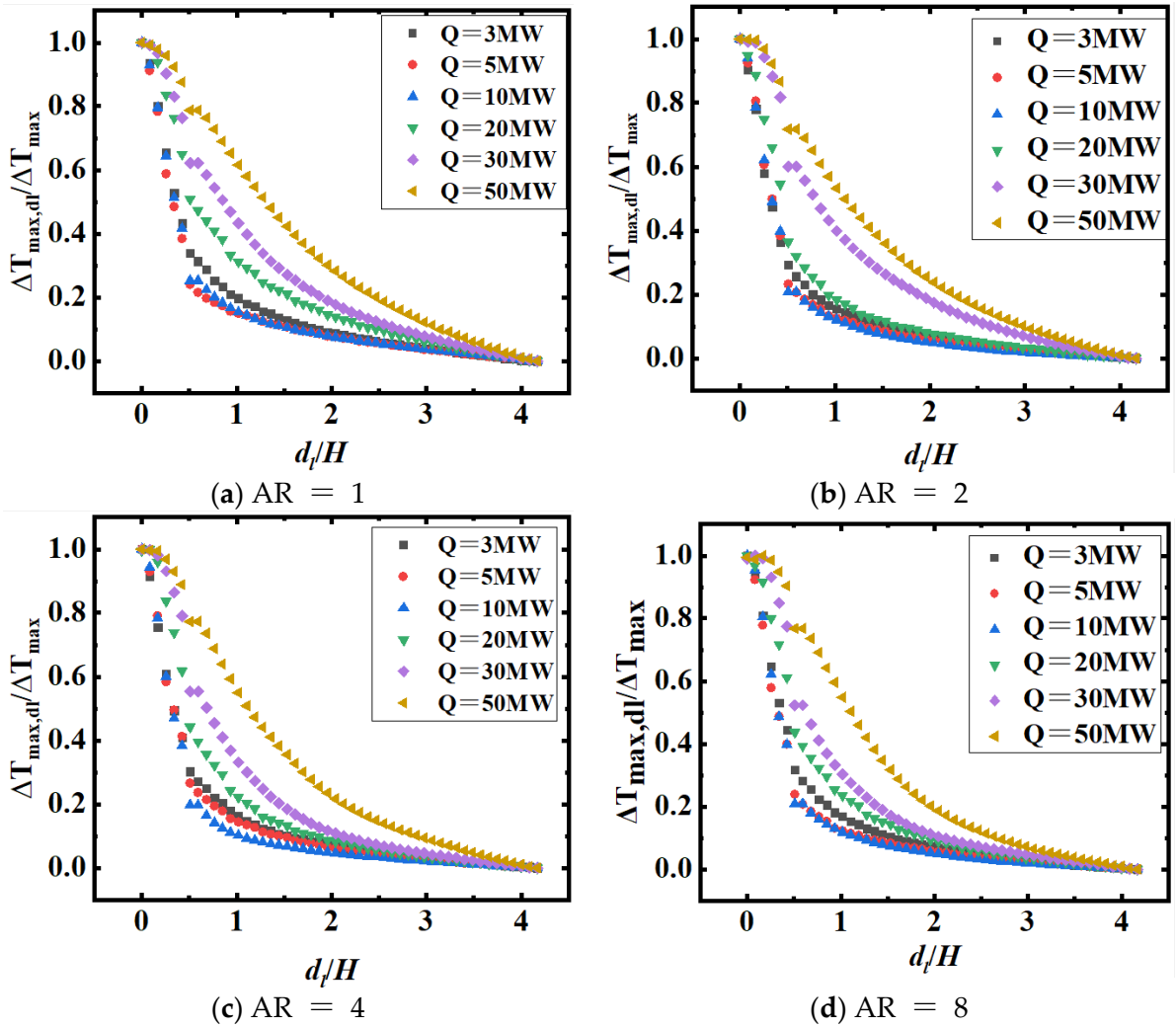

Figure 9. Dimensionless longitudinal temperature under the ceiling with various conditions.

Figure 10 demonstrates that the dimensionless longitudinal temperature for weak plumes is accurately linked using Equation (13). The parameters used for fitting are summarized in Table 1. All of the adjusted R-squared values are more than 0.96, indicating a highly satisfactory match. It is evident that coefficient *A* has a maximum variation of 3% and coefficient *B* has a maximum divergence of 9% as the tunnel cross aspect ratio increased from one to eight. Nevertheless, coefficient *C* exhibited a significant decrease of 31.7% when the tunnel aspect ratio increased from one to eight. Thus, coefficients *A* and *B* were averaged to simplify the connection. Coefficient *C* was determined by measuring the tunnel width, as shown in Equation (15).

$$C = 0.09652e^{-AR/0.48438} + 0.0297 \quad (15)$$

Substituting Equation (15) into Equation (13), the final correlation of the longitudinal temperature distribution for weak plumes can be derived; see Equation (16).

$$\frac{\Delta T_x}{\Delta T_{\max}} = 1.02e^{(-2.33\frac{x}{H})} + 0.0965e^{-AR/0.48438} + 0.0297 \quad (16)$$

Table 1. All the fitting coefficients with different tunnel aspect ratios.

AR	*A*	*B*	*C*	Adj-R^2
1	1.00022	0.45719	0.04195	0.96
2	1.02938	0.41419	0.0312	0.97
4	1.02412	0.42393	0.03081	0.98
8	1.03699	0.42914	0.02866	0.96

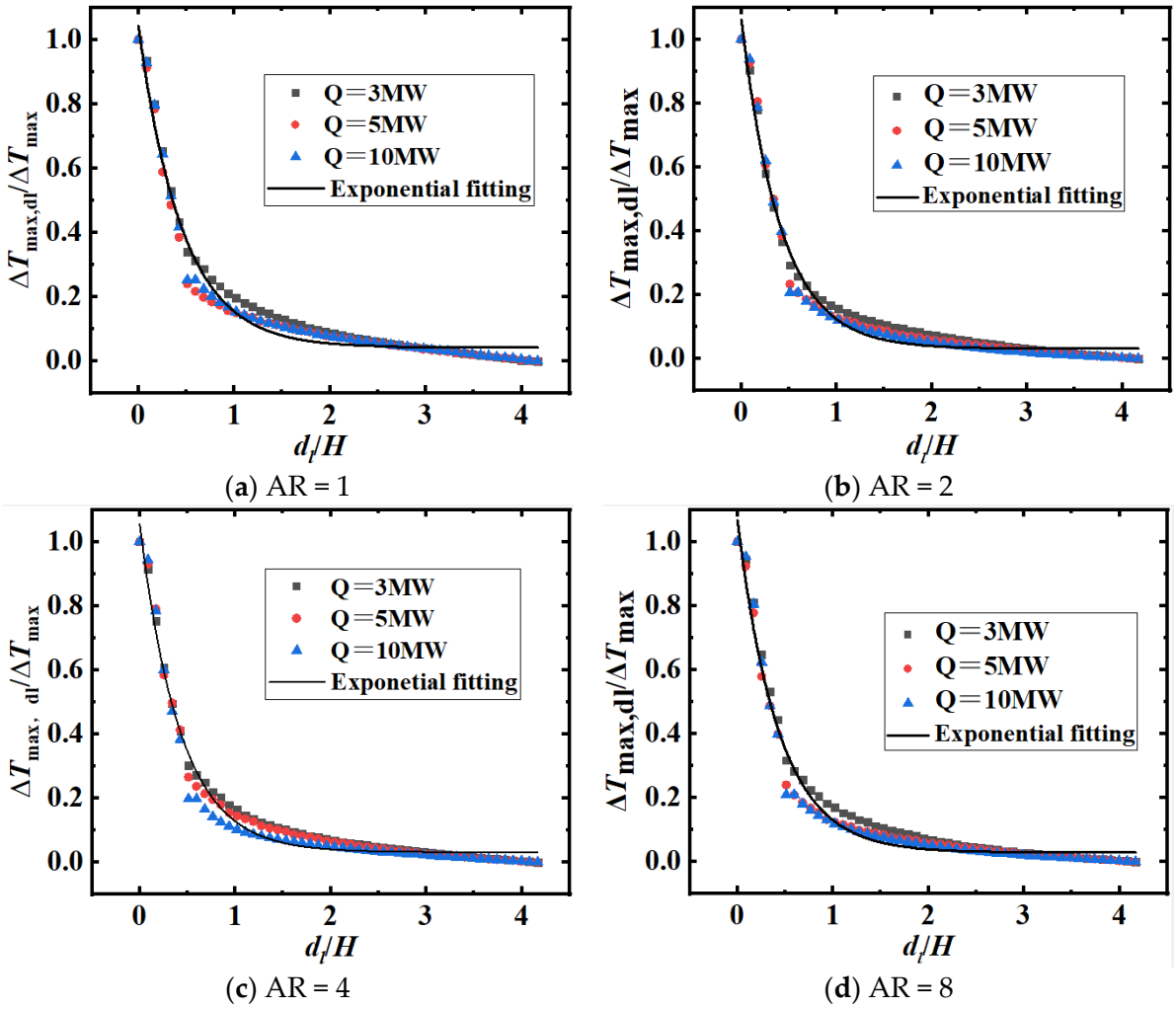

Figure 10. Longitudinal temperature decay correlations for weak plumes.

Figure 11 shows the fitting relationship of the longitudinal temperature distribution driven by strong plumes with different conditions. The decay rate of dimensionless longitudinal temperature exhibits a noticeable difference when subjected to varying heat release rates. The coefficients in Equation (14) were derived through the process of fitting the data under different situations. To build a model that accurately predicts the longitudinal temperature distribution driven by strong plumes, the obtained coefficients *A*, *B*, and *C* were plotted in Figures 12–14, respectively. Coefficient *A* is presented linearly with *Q* for different ARs. The slopes derived from different ARs remain rather consistent, as seen in Figure 12a. However, the intercept exhibits a non-linear rise as the AR increases, as depicted in Figure 12b. By substituting the appropriate equation found into the connection between *Q* and *A* in Figure 12a, the expression for *A* was determined as Equation (17). Furthermore, the correlation between coefficient *B*, as shown in Figure 10, was determined and can be expressed as Equation (18). Coefficient *C* has a negative correlation with the

growing Q, but it demonstrates a nearly constant relationship with AR, as seen in Figure 14. Correlation coefficient C can be expressed as Equation (19).

$$A = 0.0024Q^* - 0.103 \times 0.589^{AR} + 1.018 \tag{17}$$

$$B = \left(0.00235 - 7.18 \times 10^{-4} AR\right) Q^* \tag{18}$$

$$C = 0.116 - 0.0027Q^* \tag{19}$$

Then, substituting Equations (17)–(19) into Equation (14), the ultimate model for the longitudinal temperature distribution caused by powerful plumes was derived. The model can be expressed as follows:

$$\frac{\Delta T_x}{\Delta T_{\max}} = \left(0.0024Q^* - 0.103 \times 0.589^{AR} + 1.018\right) e^{\left(-\frac{d_l}{H}\right)/\left[(0.00235 - 7.18 \times 10^{-4} AR)Q^*\right]} + 0.116 - 0.0027Q^* \tag{20}$$

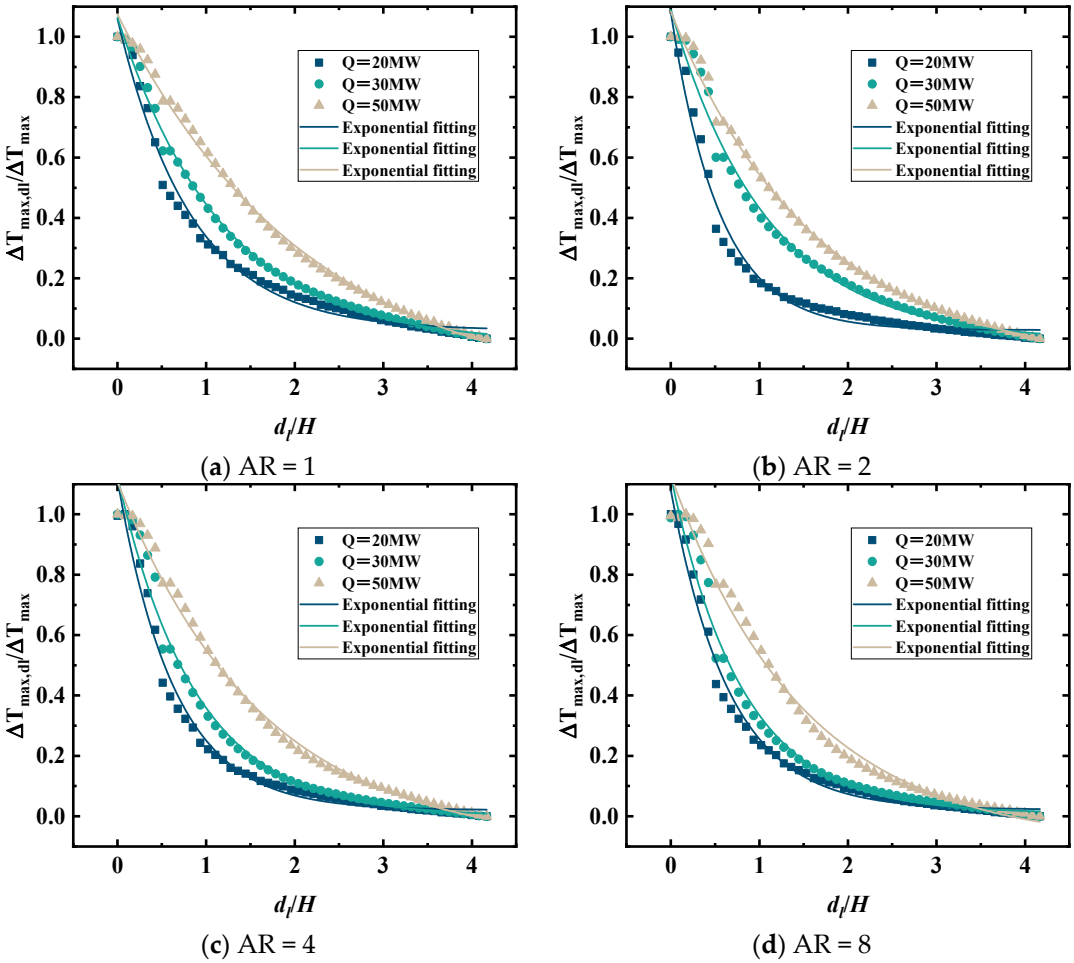

Figure 11. Longitudinal temperature decay correlations for strong plumes.

The predictions of the longitudinal temperature proposed model were compared with the simulation result as well as the previous model, as shown in Figure 15. It can be seen that the simulation results are in good agreement with the predicted values. However, Ji's model [21] underestimates longitudinal temperature profiles in the far field of the fire source. The reason for this may be that Ji's model only considers the near-field temperature of the fire source.

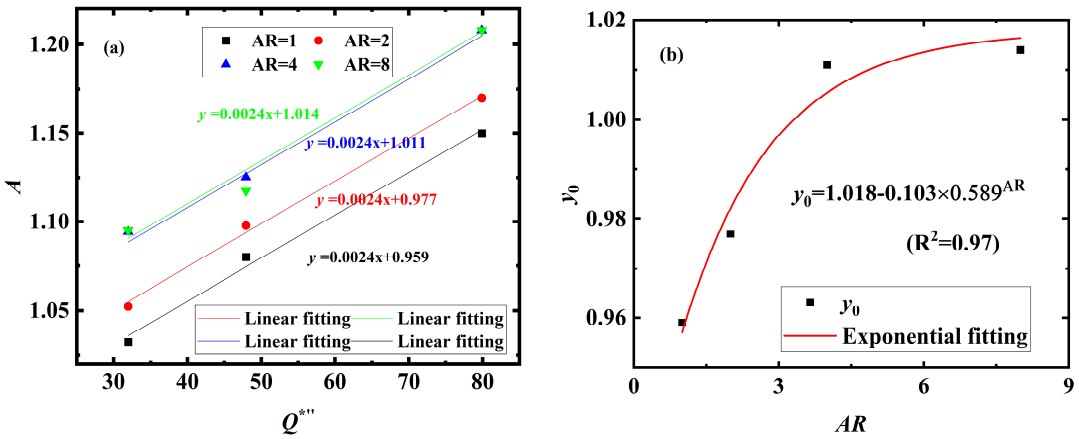

Figure 12. The fitting relationship of coefficient *A* (**a**) and y_0 (**b**).

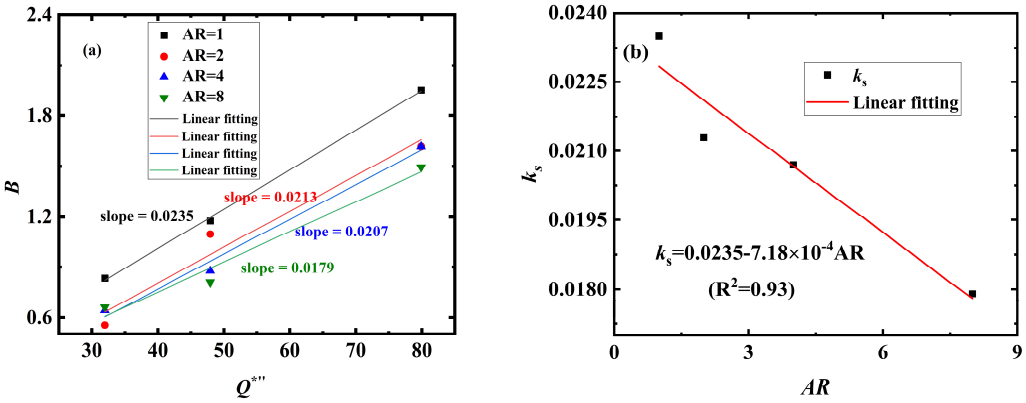

Figure 13. The fitting relationship of coefficient *B* (**a**) and k_s (**b**).

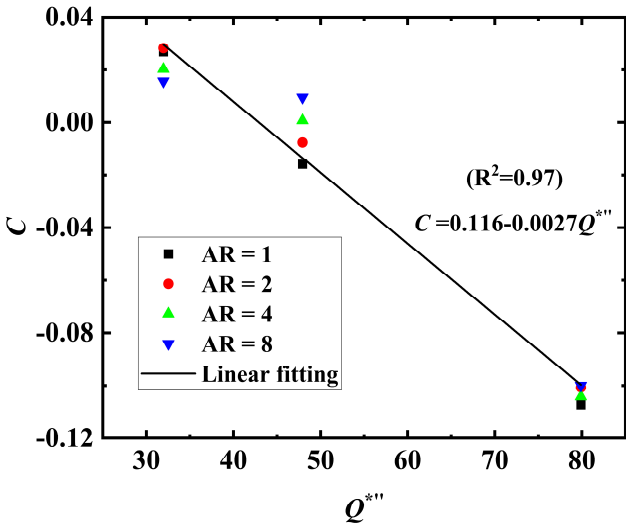

Figure 14. The fitting relationship of coefficient *C*.

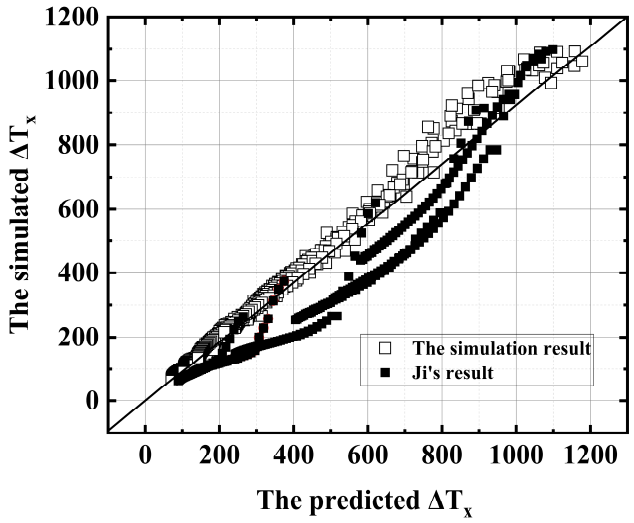

Figure 15. Comparison of the simulated value of ΔT_x with the predicted one in this work as well as the previous result [21].

4. Conclusions

The temperature distribution in a tunnel with varying tunnel aspect ratios was the subject of comparative studies in this work, which were driven by weak and strong plumes. The primary focus of the investigation and quantification was the impact of the tunnel aspect ratio on temperature distribution. Two formulas were devised to forecast the maximum excess temperature and longitudinal temperature decay. The primary conclusions are as follows:

(1) The aspect ratio of the tunnel has a minimal impact on the temperature distribution near the fire area, but it has a significant influence on the temperature distribution far away from the fire source. As the tunnel's aspect ratio increases, the temperature under the ceiling decreases.

(2) An empirical model was developed to predict the dimensionless maximum excess temperature by introducing a characteristic fire source diameter based on Ji's correlation.

(3) The far-field temperature gradient of the fire source shows a non-monotonic trend with distance. The decreasing gradient of the temperature distribution induced by a strong plume is greater than that induced by a weak plume.

(4) The influence of HRR on the attenuation behavior of longitudinal temperature can be ignored under weak plume conditions, while the influence of HRR on the decay behavior of longitudinal temperature is greater under strong plume conditions. Consequently, the correlations of longitudinal temperature decay driven by weak and strong plumes were established, respectively, with tunnel aspect ratios being considered.

In this paper, the findings may offer valuable insights to researchers seeking a deeper understanding of fire growth and the evolution of ceiling temperature in tunnel fires, whether characterized by weak or strong plumes. The analysis could guide the design of fire detection and alarm devices. However, it should be noted that only four tunnel aspect ratios and seven HRRs were selected to investigate the maximum temperature under the ceiling. Therefore, engineers should examine its application scope before designing tunnel fire prevention and control. In addition, more and more ultra-wide cross-section subsea tunnels have been built in China in recent years, such as the deep-middle channel. Lateral centralized smoke extraction is one of the most commonly used methods in subsea tunnels. The characteristics and control of smoke migration under the coupling of lateral concentrated smoke exhaust and cross-sections of different sizes may be one of the areas future research addresses.

Author Contributions: Methodology, Z.L., G.L. and D.X.; Software, X.L. and D.X.; Validation, Z.L., Y.C., G.L. and B.L.; Formal analysis, Z.L., X.L., Y.C., G.L., D.X., W.H., R.Z. and B.L.; Investigation, X.L. and R.Z.; Resources, Z.L., Y.C., W.H., R.Z. and B.L.; Data curation, W.H.; Writing—original draft, X.L.; Writing—review & editing, Z.L., W.H. and B.L. All authors have read and agreed to the published version of the manuscript.

Funding: This research was funded by the National and Regional Research Center of the "Belt and Road" of the National Ethnic Affairs Commission-Japan Emergency Management Research Center under Grant No. 2024RBYJGL-3; the Natural Science Foundation of Hebei Province under Grant No. E2020402036; the Innovation Fund Project of Hebei University of Engineering under Grant No. SJ2401002066; and the Innovation Cultivation Fund Project of Hebei University of Engineering under Grant No. SJ2401405532. The authors confirm that there are no conflicts of interest related to the publication of this paper.

Institutional Review Board Statement: Not applicable.

Informed Consent Statement: Not applicable.

Data Availability Statement: The original contributions presented in the study are included in the article, further inquiries can be directed to the corresponding author.

Conflicts of Interest: Author Gang Li was employed by the company Sinosteel Maanshan General Institute of Mining Research Co., Ltd. The remaining authors declare that the research was conducted in the absence of any commercial or financial relationships that could be construed as a potential conflict of interest.

References

1. Ji, J.; Guo, F.; Gao, Z.; Zhu, J. Effects of ambient pressure on transport characteristics of thermal-driven smoke flow in a tunnel. *Int. J. Therm. Sci.* **2018**, *125*, 210–217. [CrossRef]
2. Wan, H.; Gao, Z.; Ji, J.; Fang, J.; Zhang, Y. Experimental study on horizontal gas temperature distribution of two propane diffusion flames impinging on an unconfined ceiling. *Int. J. Therm. Sci.* **2019**, *136*, 1–8. [CrossRef]
3. Karlsson, B.; Quintiere, J. *Enclosure Fire Dynamics*; CRC Press: Boca Raton, FL, USA, 1999.
4. Tao, H.; Xu, Z.; Zhang, Y.; Zhang, X.; Fan, C. An experimental study on the smoke spread in underground interconnected infrastructure with longitudinal ventilation. *Tunn. Undergr. Space Technol.* **2023**, *142*, 105381. [CrossRef]
5. Li, L.; Cheng, X.; Wang, X.; Zhang, H. Temperature distribution of fire-induced flow along tunnels under natural ventilation. *J. Fire Sci.* **2011**, *2*, 16. [CrossRef]
6. Hu, L.H.; Huo, R.; Peng, W.; Chow, W.K.; Yang, R.X. On the maximum smoke temperature under the ceiling in tunnel fires. *Tunn. Undergr. Space Technol.* **2006**, *21*, 650–655. [CrossRef]
7. Caliendo, C.; Genovese, G.; Russo, I. A Simultaneous Analysis of the User Safety and Resilience of a Twin-Tube Road Tunnel. *Appl. Sci.* **2022**, *12*, 3357. [CrossRef]
8. Gao, Z.; Li, L.; Sun, C.; Zhong, W.; Yan, C. Effect of longitudinal slope on the smoke propagation and ceiling temperature characterization in sloping tunnel fires under natural ventilation. *Tunn. Undergr. Space Technol.* **2022**, *123*, 104396. [CrossRef]
9. Ding, H.; Quintiere, J.G. An integral model for turbulent flame radial lengths under a ceiling. *Fire Saf. J.* **2012**, *52*, 25–33. [CrossRef]
10. Alpert, R.L. Turbulent Ceiling-Jet Induced by Large-Scale Fires. *Combust. Sci. Technol.* **1975**, *11*, 197–213. [CrossRef]
11. Chen, L.; Tang, F.; Pang, H. Ceiling heat flux and downward received radiation heat flux induced by weak and relative strong fire plume in ventilation tunnels. *Appl. Therm. Eng.* **2020**, *169*, 114924. [CrossRef]
12. Heskestad, G. Engineering Relations for Fire Plumes. *Fire Saf. J.* **1984**, *7*, 25–32. [CrossRef]
13. Mccaffrey, B.J. *Purely Buoyant Diffusion Flames: Some Experimental Results*; National Institute of Standards and Technology: Gaithersburg, MD, USA, 1979; NBSIR 79–1910.
14. Hurley, M.J. *SFPE Handbook of Fire Protection Engineering*, 5th ed.; Springer: New York, NY, USA, 2016.
15. Yi, L.; Niu, J.L.; Xu, Z.S.; Wu, D.X. Experimental studies on smoke movement in a model tunnel with longitudinal ventilation. *Tunn. Undergr. Space Technol.* **2013**, *35*, 135–141. [CrossRef]
16. Zhang, X.; Hu, L.; Zhu, W.; Zhang, X.; Yang, L. Flame extension length and temperature profile in thermal impinging flow of buoyant round jet upon a horizontal plate. *Appl. Therm. Eng.* **2014**, *73*, 15–22. [CrossRef]
17. Gao, Z.H.; Liu, Z.X.; Wan, H.X.; Zhu, J.P. Experimental study on longitudinal and transverse temperature distribution of sidewall confined ceiling jet plume. *Appl. Therm. Eng.* **2016**, *107*, 583–590. [CrossRef]
18. Tang, F.; Hu, P.; Wen, J. Experimental investigation on lateral ceiling temperature distribution induced by wall-attached fire with various burner aspect ratios in underground space. *Fire Saf. J.* **2021**, *120*, 103055. [CrossRef]
19. Zhou, T.; Zhou, Y.; Fan, C.; Wang, J. Experimental study on temperature distribution beneath an arced tunnel ceiling with various fire locations. *Tunn. Undergr. Space Technol.* **2020**, *98*, 103344. [CrossRef]

20. Li, Z.; Gao, Y.; Li, X.; Mao, P.; Zhang, Y.; Jin, K.; Li, T.; Chen, L. Effects of transverse fire locations on flame length and temperature distribution in a bifurcated tunnel fire. *Tunn. Undergr. Space Technol.* **2021**, *112*, 103893. [CrossRef]
21. Ji, J.; Bi, Y.; Venkatasubbaiah, K.; Li, K. Influence of aspect ratio of tunnel on smoke temperature distribution under ceiling in near field of fire source. *Appl. Therm. Eng.* **2016**, *106*, 1094–1102. [CrossRef]
22. Xu, Z.; Zhao, J.; Liu, Q.; Chen, H.; Liu, Y.; Geng, Z.; He, L. Experimental investigation on smoke spread characteristics and smoke layer height in tunnels. *Fire Mater.* **2019**, *43*, 303–309. [CrossRef]
23. Lee, S.R.; Ryou, H.S. An experimental study of the effect of the aspect ratio on the critical velocity in longitudinal ventilation tunnel fires. *J. Fire Sci.* **2005**, *23*, 119–138. [CrossRef]
24. Li, Y.Z.; Ingason, H. Effect of cross section on critical velocity in longitudinally ventilated tunnel fires. *Fire Saf. J.* **2017**, *91*, 303–311. [CrossRef]
25. Zhang, T.; Wang, G.; Hu, H.; Huang, Y.; Zhu, K.; Wu, K. Study on temperature decay characteristics of fire smoke backflow layer in tunnels with wide-shallow cross-section. *Tunnel. Undergr. Space Technol.* **2021**, *112*, 103874. [CrossRef]
26. Zhang, T.; Wang, G.; Li, J.; Huang, Y.; Zhu, K.; Wu, K. Experimental study of back-layering length and critical velocity in longitudinally ventilated tunnel fire with various rectangular cross-sections. *Fire Saf. J.* **2021**, *126*, 103483. [CrossRef]
27. Mcgrattan, K.; Hostikka, S.; Mcdermott, R.; Floyd, J.; Weinschenk, C.; Overholt, K. *Fire Dynamics Simulator User's Guide*; National Institute of Standards and Technology: Gaithersburg, MD, USA, 2016.
28. Jiang, X.; Chen, X.; Xiao, N.; Liao, X.; Fan, C. Influence of the competitive effect of V-shaped slope tunnel on smoke characteristics. *Tunnel. Undergr. Space Technol.* **2021**, *118*, 104193. [CrossRef]
29. Yao, Y.; Qu, B.; Zhu, H.; Wang, J.; Zhao, S.; Wang, Q. Theoretical and numerical study on critical velocity and driving force for preventing smoke backlayering in a connection roadway fire of coal mines. *Tunn. Undergr. Space Technol.* **2022**, *127*, 104566. [CrossRef]
30. Wang, Y.; Sun, X.; Liu, S.; Yan, P.; Qin, T.; Zhang, B. Simulation of back-layering length in tunnel fire with vertical shafts. *Appl. Therm. Eng.* **2016**, *109*, 344–350. [CrossRef]
31. Zhang, X.; Lin, Y.; Shi, C.; Zhang, J. Numerical simulation on the maximum temperature and smoke back-layering length in a tilted tunnel under natural ventilation. *Tunnel. Undergr. Space Technol.* **2021**, *107*, 103661. [CrossRef]
32. Xu, Z.; Xu, W.; He, L.; Xie, E.; Wang, T.; Tao, H. Numerical study on the smoke extraction efficiency and the improvement through a smoke reservoir in the naturally ventilated tunnel with vertical shaft. *Tunn. Undergr. Space Technol.* **2020**, *103*, 103505. [CrossRef]
33. Li, Z.; Jiang, H.; Gao, Y.; Jin, K.; Zhang, Y.; Li, T. Study on flow characteristics of fire smoke in bifurcated tunnel. *J. Saf. Sci. Technol.* **2021**, *5*, 5. (In Chinese)
34. Wan, H.X.; Gao, Z.H.; Han, J.Y.; Ji, J.; Ye, M.J.; Zhang, Y.M. A numerical study on smoke back-layering length and inlet air velocity of fires in an inclined tunnel under natural ventilation with a vertical shaft. *Int. J. Therm. Sci.* **2019**, *138*, 11. [CrossRef]
35. Yao, Y.; Li, Y.Z.; Ingason, H.; Cheng, X. Numerical study on overall smoke control using naturally ventilated shafts during fires in a road tunnel. *Int. J. Therm. Sci.* **2019**, *140*, 491–504. [CrossRef]
36. Hai, S.; Zhu, S.; He, F.; Xiang, C.; She, J.; Li, G.; Yuan, W.; Bian, H. *Shanghai Construction Specifications (DG TJ 08-2033-2017 J11197-2017): Road Tunnel Design Standards*; Tongji University Press: Shanghai, China, 2017.
37. Shanghai Tunnel Engineering Rail Transit Design and Research Institute. *Road Tunnel Design Code, DGTJ08-2033-2017, J11197-2017*; Tongji University Press: Shanghai, China, 2017.
38. Wang, K.-h.; Liu, Y.-q.; Zhang, P.-h.; Guo, Y.-l. Numerical study on the impact of wall thermal inertia on maximum smoke temperature and longitudinal attenuation in long channel fires. *Int. J. Therm. Sci.* **2023**, *184*, 107940. [CrossRef]
39. Ji, J.; Fu, Y.; Li, K.; Sun, J.; Fan, C.; Shi, W. Experimental study on behavior of sidewall fires at varying height in a corridor-like structure. *Proc. Combust. Inst.* **2015**, *35*, 2639–2646. [CrossRef]
40. Gao, Z.H.; Ji, J.; Fan, C.G.; Sun, J.H.; Zhu, J.P. Influence of sidewall restriction on the maximum ceiling gas temperature of buoyancy-driven thermal flow. *Energy Build.* **2014**, *84*, 13–20. [CrossRef]

Disclaimer/Publisher's Note: The statements, opinions and data contained in all publications are solely those of the individual author(s) and contributor(s) and not of MDPI and/or the editor(s). MDPI and/or the editor(s) disclaim responsibility for any injury to people or property resulting from any ideas, methods, instructions or products referred to in the content.